Comprehensive Identification of Post-translational Modifications of Rat Bone Osteopontin by Mass Spectrometry†

Mandana Keykhosravani,‡,§ Amanda Doherty-Kirby,‡,|| Cunjie Zhang,|| Dyanne Brewer,⊥ Harvey A. Goldberg,§,|| Graeme K. Hunter,*,§,|| and Gilles Lajoie*,||

CIHR Group in Skeletal Development and Remodeling, School of Dentistry, and Department of Biochemistry, The University of Western Ontario, London, Ontario, N6A 5C1, Canada, and Department of Molecular Biology and Genetics, University of Guelph, Ontario, N1G 2W1, Canada

Received January 19, 2005; Revised Manuscript Received March 9, 2005

ABSTRACT: Osteopontin (OPN) is a highly modified protein that is found in many tissues and has been associated with a variety of physiological and pathological processes. Bone OPN is a potent inhibitor of hydroxyapatite crystal formation and stimulates bone resorption by osteoclasts; these activities, as well as others, are dependent upon phosphorylation of the protein. We have used mass spectrometry (MS) to perform a comprehensive analysis of the post-translational modification of OPN purified from rat bone. Matrix-assisted laser desorption time-of-flight (MALDI−TOF) MS showed masses of 37.6 and 36.8 kDa before and after enzymatic dephosphorylation, respectively, corresponding to a content of approximately 10.4 phosphate groups. Using proteolytic digestion and tandem MS, we localized 29 sites of phosphorylation: S10, S11, S46, S47, T50, S60, S62, S65, S146, T154, S160, S164, S167, S193, S196, S203, S220, S223, S232, S241, S245, S257, S262, S267, S278, S290, S295, S296, and S297. In addition, Y150 was shown to be sulfated and T107, T110, T116, and T121 are O-glycosylated. No glycan was detected at the potential N-glycosylation site. Other modifications, including deamidation, oxidation, and carbamylation, are also present. A 36-amino acid sequence from residues 67−102 could not be analyzed in detail, even after sialidase treatment, presumably because of the presence of a large number of acidic residues. In comparison to the previously characterized cow milk isoform, rat bone OPN is sulfated and has an additional site of glycosylation, many different sites of phosphorylation, and a lower overall phosphate content.

Osteopontin (OPN)[1] is a sialic acid-rich glycophosphoprotein that is rich in the amino acids aspartic acid, glutamic acid, and serine. It consists of a single chain of 264−301 amino acids, depending upon the species, and has been shown to be post-translationally modified by phosphorylation and glycosylation. OPN was first isolated from epithelial and fibroblastic cells that had undergone malignant transformation (*1*). Subsequently, a similar protein was isolated from the mineralized matrix of bovine bone and called sialoprotein I (*2*). Later, the same group determined the primary structure of sialoprotein I by sequencing cDNA prepared from rat osteosarcoma cells (ROS 17/2.8) (*3*). OPN has since been isolated from many tissues, cells, and body fluids, including kidney (*4*), placenta, smooth muscle cells (*5*), macrophages (*6*), blood, urine, and milk (*7*).

OPN has been implicated in a variety of physiological and pathological processes. It has both pro-inflammatory (*8*, *9*) and anti-inflammatory (*10*, *11*) effects. Expression of OPN is positively correlated with malignant transformation of cells and metastasis of tumors (*12*−*15*). The RGD (arginine−glycine−aspartic acid) sequence of OPN promotes attachment of osteoclasts to bone matrix via the $\alpha_v\beta_3$ integrin (vitronectin receptor) (*16*). OPN also regulates osteoclast function by effects on intracellular signaling pathways (*17*). OPN is strongly associated with a variety of forms of pathological calcification. It occurs at high levels at such sites of ectopic calcification as atherosclerotic plaque (*18*), kidney stones (*19*), dental plaque (*20*), and tumor-associated calcification (*21*). *In vitro* studies have shown that OPN strongly inhibits the formation of hydroxyapatite (calcium phosphate), the mineral phase of bones, teeth, and atherosclerotic plaque (*22*−*24*), as well as calcium oxalate, the principal mineral phase of kidney stones (*25*, *26*).

† This work was supported by a grant from the Canadian Institutes of Health Research (CIHR) to G.K.H. and by a grant from the Ontario Research and Development Challenge Fund (ORDCF) to G.L.

* To whom correspondence should be addressed. Telephone: (519) 661-2185. Fax: (519) 850-2459. E-mail: graeme.hunter@fmd.uwo.ca (G.K.H.); Telephone: (519) 661-3054. Fax: (519) 661-3954. E-mail: glajoie@uwo.ca (G.L.).

‡ These authors contributed equally to the work.

§ School of Dentistry, The University of Western Ontario.

|| Department of Biochemistry, The University of Western Ontario.

⊥ University of Guelph.

[1] Abbreviations: OPN, osteopontin; MALDI−TOF, matrix-associated desorption time-of-flight; MS, mass spectrometry; ESI, electrospray ionization; ACTH, adenocorticotrophic hormone clip 18−39; SDS−PAGE, sodium dodecyl sulfate−polyacrylamide gel electrophoresis; Q-TOF, quadrupole time-of-flight; DDA, data-dependent acquisition; PID, parent-ion discovery; FA, formic acid; HPLC, high-performance liquid chromatography; CE, collision energy; FPLC, fast protein liquid chromatography; MS/MS, tandem mass spectrometry; *H*, hexose; *N*, *N*-acetylhexosamine, *S*, sialic acid; EDTA, ethylenediaminetetraacetic acid; CID, collision-induced decomposition, APMSF, *p*-amidinophenylmethylsulfonyl fluoride.

10.1021/bi050109p CCC: $30.25
Published on Web 04/13/2005

A number of the properties of OPN have been shown to be phosphorylation-dependent. Enzymatic dephosphorylation of rat bone and chicken eggshell OPN abolishes their ability to inhibit the formation of hydroxyapatite and calcite (calcium carbonate), respectively (*22*, *23*, *27*). Likewise, recombinant OPN expressed in bacteria does not inhibit the calcification of vascular smooth muscle cell cultures unless it is phosphorylated with protein kinase CK2 (*28*). Synthetic phosphopeptides corresponding to sequences in OPN inhibit the formation of calcium oxalate (*29*) and hydroxyapatite (*30*) to far greater extents than the corresponding nonphosphorylated peptides.

The effects of OPN on bone cells have also been shown to require phosphorylation of the protein. Phosphorylation of recombinant OPN expressed in bacteria increases the adhesion of osteoclasts (*31*), whereas dephosphorylation of native OPN with acid phosphatase has the opposite effect (*32*). More highly phosphorylated forms of OPN cause greater activation of osteoclast-mediated bone resorption (*33*). These effects on osteoclasts appear to involve phosphorylation of specific residues. Phosphorylation of recombinant OPN with protein kinase CK2 promotes osteoclast attachment, but phosphorylation to a similar level with protein kinase C does not (*31*).

Some of the effects of OPN on immune cells are also affected by the number or location of phosphate groups. Phosphorylation of OPN was shown to be necessary for migration (*34*) and interleukin production (*35*) by macrophages. Recombinant OPN phosphorylated with protein kinases CK1 and CK2 or Golgi casein kinase increases the haptotaxis and chemotaxis of macrophages, whereas phosphorylation with protein kinases A or G only increases chemotaxis (*34*).

The only form of OPN to have its phosphorylation sites completely mapped is that from bovine milk. Using mass spectrometry (MS) and Edman degradation, it was shown that milk OPN is phosphorylated at 27 serine and 1 threonine residues (*36*). The authors reported the sites of potential phosphorylation to be occupied or unoccupied (i.e., there was no heterogeneity observed).

The phosphorylation sites of the rat bone isoform were partially analyzed using MS to identify the phosphopeptides generated by endoproteinase Lys-C digestion, followed by sequencing of modified peptides using Edman degradation (*37*). Peptides with identical sequence but different phosphate content were isolated, indicating that phosphorylation of rat bone OPN is heterogeneous. Phosphate groups were assigned to serine residues 10, 11, 46, 47, 295, 297, and 298. Threonine 154 and serines 160, 250, 257, and 262 were reported as "likely" phosphorylated. No results were obtained for the sequence 55−139.

Forms of OPN differing in phosphate content occur within as well as between tissues. Highly and poorly phosphorylated forms of OPN have been isolated from a number of tissues or cell cultures, including epidermal cells and fibroblasts (*4*), kidney cells (*38*), osteosarcoma cell lines (*39*), and bone (*40*).

In addition to phosphorylation, osteopontin has been reported to be both glycosylated and sulfated. Bovine milk OPN has three O-linked glycans (*36*), while an earlier study of rat bone OPN postulated one N-linked and five to six O-linked oligosaccharides present (*41*). Another group has reported that PNGase F digestion of OPN secreted by the tsB77 (a rat-1 cell line from fibroblasts) does not alter migration of the protein on gels, suggesting that no N-linked glycans are present (*42*). Rat bone OPN contains sulfate that was not removed by deglycosylation, indicating that the sulfate was associated with the polypeptide and not the glycans. However, the site of this modification was not identified (*43*).

In view of the well-characterized effects of OPN on rat osteoclast adhesion and resorption and because rat bone OPN has been used most commonly in studies on crystal formation, it is of great interest to determine the exact pattern of phosphorylation of this isoform. In the present study, we use MS to identify 29 sites of phosphorylation, 1 site of sulfation, and 4 sites of O-glycosylation in rat bone OPN.

MATERIALS AND METHODS

Materials. The following items were purchased: APMSF from Calbiochem (San Diego, CA), human thrombin, endoproteinase Asp-N, equine cytochrome *c*, bovine trypsinogen, bovine serum albumin, α-hydroxycinnamic acid, sinapinic acid, adenocorticotrophic hormone clip 18−39 (ACTH), angiotensin I, renin substrate *β-N*-acetylglucosaminidase (sialidase A, recombinant from *Streptococcus pneumonia*), EDTA, and guanidine-HCL from Sigma (Mississauga, ON, Canada), sequencing-grade trypsin from Promega (Madison, WI), calf intestinal alkaline phosphatase from New England Biolabs (Mississauga, ON, Canada), fast protein liquid chromatography (FPLC) chromatography columns and resins, 12.5% polyacrylamide electrophoresis gels, and SDS buffer strips, from Amersham Pharmacia Biotech (Montreal, QC, Canada), HPLC-grade acetonitrile, water, and formic acid from Fisher, C18 nano-LC analytical and C4 micro columns from LC Packings (Dionex), and C18 microcolumns from Agilent. The ProteoSpin Detergent Cleanup Micro Kit was received as a trial sample from MDS-Sciex (Concord, ON, Canada). All chemicals used were Analar-grade or better. All water used for reactions was of Milli-Q quality or HPLC-grade.

Isolation of OPN from Rat Bone. Native rat bone OPN was purified as previously described (*44*). In brief, approximately 100 g (wet weight) of adult rat long bone was washed with phosphate-buffered saline solution containing proteinase inhibitors then ground with a mortar and pestle under liquid nitrogen. The resulting powder was treated with 4.0 M guanidine-HCl to remove nonmineral-associated proteins and then treated with 0.5 M EDTA. The EDTA extract was concentrated by ultrafiltration, subjected to buffer exchange, and purified by FPLC on Q Sepharose Fast Flow and Superdex 200 PG columns. The yield and purity of protein were determined by amino acid analysis (Alberta Peptide Institute) and SDS−PAGE with Stains All/silver staining (*45*). The putative OPN band at ∼66 kDa on SDS−PAGE was not detectable after digestion with thrombin, indicating that contamination with other proteins was insignificant (*7*). All protein amounts mentioned below are based on amino acid analysis.

Analysis of Full-Length Rat Bone OPN with Matrix-Assisted Desorption Time-of-Flight (MALDI−TOF) and ESI−MS. MS analysis of intact full-length bone OPN was performed using a Reflex III MALDI−TOF instrument (Bruker, Germany) equipped with a 337-nm nitrogen laser

in a linear and positive-ion mode. Samples (2 μg each) were combined with a saturated solution of sinapinic acid in 50% acetonitrile/0.1% trifluoroacetic acid and spotted onto the MALDI plate in duplicate. The plate was analyzed by positioning the laser at different spots, and 300 laser shots of 90−104 μJ were summed. The instrument was externally calibrated with equine cytochrome *c*, bovine trypsinogen, and bovine serum albumin. Results were processed, and peaks were assigned using the XTOF software (Bruker, Germany). To remove phosphates present in native OPN, 37 μg of OPN was incubated with 0.04 unit of calf alkaline phosphatase in 10 mM NH_4HCO_3 at pH 8.5 overnight at 37 °C. The samples were then stored at −20 °C and analyzed by linear MALDI−TOF as described above.

Similarly, 10 μg of rat bone OPN was dephosphorylated with calf alkaline phosphatase and analyzed using ESI−MS. Online liquid chromatography−MS was performed with a microbore C4 column (1 mm × 15 cm, LC Packings) using a gradient of 5−95% B over 60 min (A = 0.1% formic acid in water, and B = 0.1% formic acid in acetonitrile) and a flow rate of 30 μL/min. ESI−MS was performed on a Q-TOF MS (Micro, Micromass) with the following parameters: source temperature, 80 °C; capillary voltage, 3.2 kV; cone voltage, 35 V; and MS data acquisition range, 500−2800. MS data were processed using the maximum entropy algorithm (MaxEnt1) (*46*) included in the manufacturer's software.

Enzymatic Digestion of Phosphorylated OPN. To generate peptides for MS analysis, 5 μg aliquots of OPN were dissolved in 10 mM NH_4HCO_3 at pH 8.0 or 50 mM NH_4HCO_3 at pH 8.5 and incubated for 18 h at 37 °C in the presence of 100 ng of sequencing-grade trypsin or 100 ng of endoproteinase Asp-N, respectively. The samples were then dried using a Savant SpeedVac Plus and redissolved in 20 μL of 0.2% formic acid.

Enzymatic Digestion of OPN for Glycosylation Analysis. To generate dephosphorylated OPN, 10 μg aliquots of OPN were dissolved in 20 μL of 100 mM NH_4HCO_3 and incubated for 45 min at 37 °C in the presence of 1 μL of calf alkaline phosphatase. The dephosphorylated but otherwise intact OPN was further purified using HPLC on a microbore C18 column, dried, and digested with trypsin or Asp-N as described above. The dephosphorylated tryptic peptides were desialylated under denaturing conditions with sialidase A using the manufacturer-supplied protocols and reagents. After the reaction, a ProteoSpin Detergent Cleanup Micro Kit was used to remove detergents from the sample. Sample aliquots were used for LC−MS analysis of large tryptic glycopeptides or subsequently digested with Asp-N and used for LC−MS/MS analysis to determine the locations and structures of glycans without sialic acid. To determine the total composition of glycans with sialic acid, an Asp-N digestion of dephosphorylated OPN was analyzed by LC−MS/MS.

Nanoscale LC−MS and LC−MS/MS. Peptides were generated with different enzymes as described above. Nano-LC/ESI/MS and MS/MS analysis was performed on a hybrid quadrupole time-of-flight mass spectrometer (Q-TOF GLOBAL Ultima, Micromass, Manchester, U.K.) using either data-dependent acquisition (DDA, automated and targeted) or parent-ion discovery (PID) modes. A capillary LC (Waters) fitted with an autosampler was used for all separations. Chromatographic separation was achieved using a ten-port switching valve, which allowed for loading of the sample onto a precolumn (0.5 × 5 mm, LC Packings) at high flow rates (30 μL/min) followed by changing the valve position for elution of the analyte from the precolumn to an analytical column (15 cm × 75 μm, 300 nL/min) that eluted directly through a nanoLC probe (Micromass) into the mass spectrometer. Solvents used were C, 0.1% formic acid (FA) in HPLC-grade water for sample loading; A, 0.1% FA in water; and B, 0.1% FA in acetonitrile for sample elution. Peptides were eluted after a 3-min loading period using a linear gradient of 5−60% B over 32 min, 60−95% B over 5 min, 95% B for 10 min, 95−5% B over 5 min, and 5% B for 10 min.

For DDA experiments, the mass spectrometer was operated in positive-ion mode using the following parameters: source temperature, 80 °C; capillary voltage, 3.2 kV; cone voltage, 45−60 V; collision energy for MS mode, 10 V; MS data acquisition range, 400−1900; MS/MS data acquisition range, 50−1900. The collision energy (CE) for MS/MS experiments was determined by the charge state of the precursor ion and/or by the *m*/*z* range of the precursor ion. The CE values were according to standard charge-state recognition and CE files recommended by Micromass. MS to MS/MS switching was allowed for the four most abundant precursors in the survey experiment, with 10 s of MS/MS data being acquired for each peptide. In some cases, specific precursor ions were targeted to undergo tandem MS using user-specified collision energies.

For PID experiments, the CE was switched alternatively between low (10 V) and high (28−30 V) every second. MS/MS data acquisition was triggered by the loss of 97.97 corresponding to the neutral loss of phosphate. For the MS and MS/MS experiments, the TOF detector was calibrated with Glu-fibrinopeptide-b. Data were acquired using MassLynx 4.0 (Micromass).

Analysis of MS Data. For each DDA or PID experiment, MS survey spectra were combined and subjected to baseline subtraction. The spectra of all charge states (*m*/*z* of +2, +3, +4, or higher) were deconvoluted into their monoisotopic $M + H^+$ species using the MaxEnt3 algorithm included in the MassLynx suite of software. Lists of $M + H^+$ species generated from the deconvoluted spectra were used to search protein databases using MASCOT (www.matrixscience.com). For a typical search, oxidation of methionine and phosphorylation of threonine or serine were given as variable modifications. The peptides reported with phosphorylation were further examined by analysis of the raw data (*m*/*z* of different charge states) and sequenced by MS/MS to localize the phosphorylation sites.

Analysis of MS/MS Data. The raw MS/MS data for DDA and PID experiments were converted to the Micromass .pkl data format using the PeptideAuto function of MassLynx or ProteinLynxGlobalServer 2.0 (Micromass). These multiple .pkl files were used to search MASCOT or used in the *de novo* sequencing software PEAKS (Bioinformatics Solutions Inc, Waterloo, ON, Canada) (*47*). In some cases, spectra corresponding to the MS/MS of individual precursor ions were manually processed and exported to Sequest format .dta files and analyzed using MASCOT or PEAKS. In all searches, oxidation and phosphorylation were specified as variable modifications. Data were also searched for deamidation, carbamylation, pyroglutamic acid formation, and

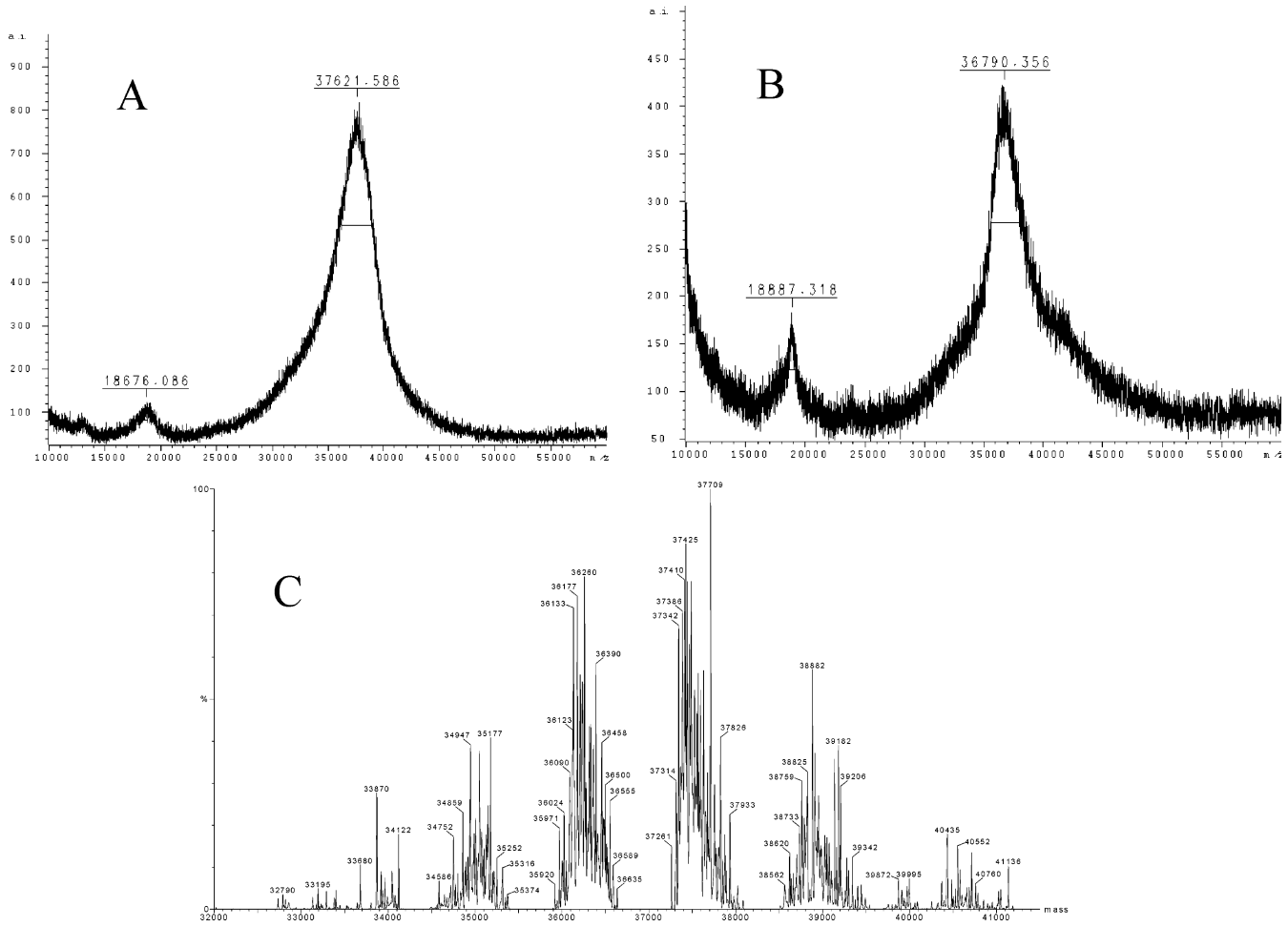

FIGURE 1: Analysis of phosphatase-treated and untreated intact OPN. Linear MALDI−MS spectra (A) prior to and (B) after treatment with calf alkaline phosphatase. The difference in average mass is approximately 831 Da, corresponding to 10.4 mol of phosphate. The mass is still significantly higher than that expected for unmodified OPN, supporting the presence of glycosylation. (C) MaxEnt 1-processed ESI−MS data for dephosphorylated rat bone osteopontin showing that the protein is still heterogeneous after phosphatase treatment. The various groups of peaks suggest heterogeneous glycosylation.

sulfation. All automated sequencing results were verified for accuracy. The glycopeptide data were interpreted manually.

RESULTS

MS Analysis of Intact Rat Bone OPN. The ESI−MS spectrum of untreated rat bone OPN was a broad raw *m*/*z* envelope without resolved peaks that could be deconvoluted, indicative of very high heterogeneity. Analysis by linear MALDI, using external calibration verified with recombinant OPN expressed in *Escherichia coli*, was also attempted. A broad peak with an average molecular mass of 37 621 Da was obtained with rat bone OPN (Figure 1A). To estimate the total number of phosphate and sugar groups present, OPN was treated with alkaline phosphatase, and the resulting protein was analyzed by MALDI on the same day as the untreated sample. The average molecular mass of dephosphorylated native OPN was 36 790 Da, which corresponds to a loss of approximately 10.4 phosphate groups (831 Da) (Figure 1B). Assuming that the dephosphorylation reaction was complete, the average mass of the other post-translational modifications (most likely glycosylation) on rat bone OPN would be 3542 Da (the theoretical average mass of the unmodified rat OPN polypeptide is 33 248 Da), corresponding to approximately 9% carbohydrate by mass, which is consistent with the results from glycopeptide analysis (see below).

ESI−MS of the dephosphorylated sample gave a complex spectrum that was deconvoluted with MaxEnt1 to give multiple species ranging from 33 to 41 kDa (Figure 1C). The variation may represent incomplete glycosylation at several residues. Within each grouping, differences of approximately 43 and 292 Da are present, likely corresponding to carbamylation (verified at the peptide level) and sialic acid, respectively.

Peptide Phosphorylation Analysis. The survey MS data obtained for the trypsin and Asp-N digests of rat bovine OPN were performed using a Q-TOF (GLOBAL) instrument. Examination of MS raw data revealed that there are multiple species for many peptides corresponding to several states of phosphorylation for each peptide. For trypsin-digested peptides, the MASCOT search indicated a total of 24 phosphates for 8 nonoverlapping peptides (Table 1). This table takes into account overlapping regions or smaller peptides with fewer missed cleavages. Peptide mapping using Asp-N indicates a total of 30 phosphates present in 11 different peptides (Table 2). When these results are taken together, the MS survey spectra of Asp-N and trypsin-digested OPN covered the full sequence with the exception of 67−128,

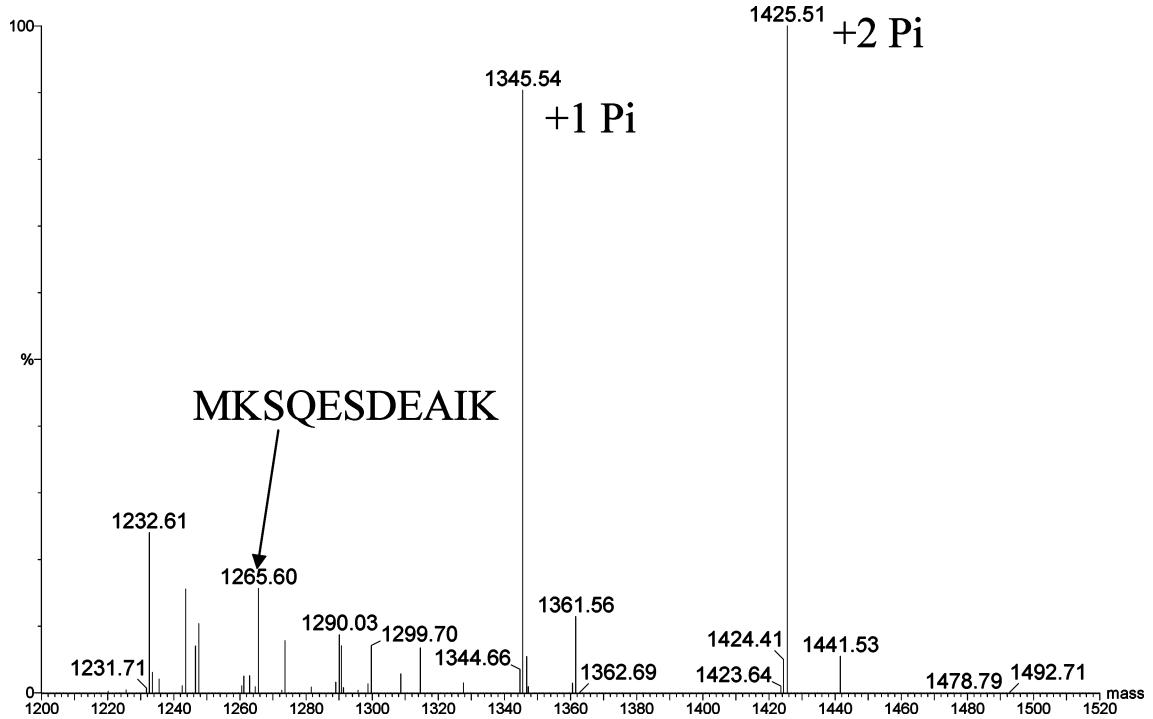

FIGURE 2: Q-TOF MS analysis of tryptic peptide MKSQESDEAIK. Processed ESI−MS data for OPN 162−172 showing the singly charged species for unmodified and phosphorylated forms. Theoretical values are 1265.60, 1345.57, and 1425.54 for the unmodified, singly, and doubly phosphorylated species. The corresponding CID MS/MS spectra are shown in Figure 3.

Table 1: Summary of Phosphorylated Peptides after Trypsin Digestion of Rat Bone OPN from LC−MS Survey Spectra

number	peptide sequence	number of S + T	putative number of phosphates
T5−19	VAEFGSSEEKAHYSK	3	2
T142−161	SFPVSDEQYPDATDEDLTSR	5	4
T162−179	MKSQESDEAIKVIPVAQR	2	2
T180−216	LSVPSDQDSNGKTSHESSQLDEPSVETHSLEQSKEYK	11	5
T217−255	QRASHESTEQSDAIDSAEKPDAIDSAERSDAIDSQASSK	10	4
T256−277	ASLEHQSHEFHSHEDKLVLDPK	3	3
T278−286	SKEDDRYLK	1	1
T287−301	FRISHELESSSSEVN	5	3

Table 2: Summary of Phosphorylated Peptides Detected after Asp-N Digestion of Rat Bone OPN from LC−MS Survey Spectra

number	peptide sequence in rat bone OPN	number of S + T	putative number of phosphates
D1−21	LPVKVAEFGSSEEKAHYSKHS	4	2
D22−50	DAVATWLKPDPSQKQNLLAPQNSVSSEET	6	3
D51−66	DDFKQETLPSNSNESH	4	3
D130−151	DSLAYGLRSKSRSFPVSDEQYP	5	2
D155−184	DEDLTSRMKSQESDEAIKVIPVAQRLSVPS	5	3
D187−199	DSNGKTSHESSQL	5	2
D200−230	DEPSVETHSLEQSKEYKQRASHESTEQSDAI	8	5
D231−239	DSAEKPDAI	1	1
D240−248	DSAERSDAI	2	1
D246−269	DAIDSQASSKASLEHQSHEFHSHE	6	5
D282−301	DRYLKFRISHELESSSSEVN	5	3

which contains 9 serine and 4 threonine residues. Using ESI−MS in positive-ion mode, no signal could be assigned to this region, and thus, sites of phosphorylation were not detected.

Tandem MS Analysis. Several MS/MS experiments were used to localize the modified sites. Because of the extensive modification of OPN (see below), experiments that employed DDA generally gave better coverage than PID experiments because of the decreased duty cycle for the PID mode. To increase coverage of the protein, both Asp-N and trypsin digests were analyzed. This MS/MS coverage with verified peptides was 59% for trypsin and 75% for Asp-N, for a combined coverage of 79%. Generally, tryptic peptides yielded better MS/MS fragmentation data than Asp-N digests. It should be noted that none of the samples was enriched for phosphopeptides by immobilized-metal-affinity chromatography prior to MS analysis because of the extremely acidic nature of OPN (75 of 301 residues are D or E) and the presence of multiply phosphorylated peptides that might be retained on an IMAC column.

From the peptide-mapping results, it is clear that OPN is heterogeneously phosphorylated. An example of this is illustrated in Figure 2, which shows three monoisotopic (1^+) species for OPN 162−172 (MKSQESDEAIK) without modification (1265.60) and with one (1345.54) or two

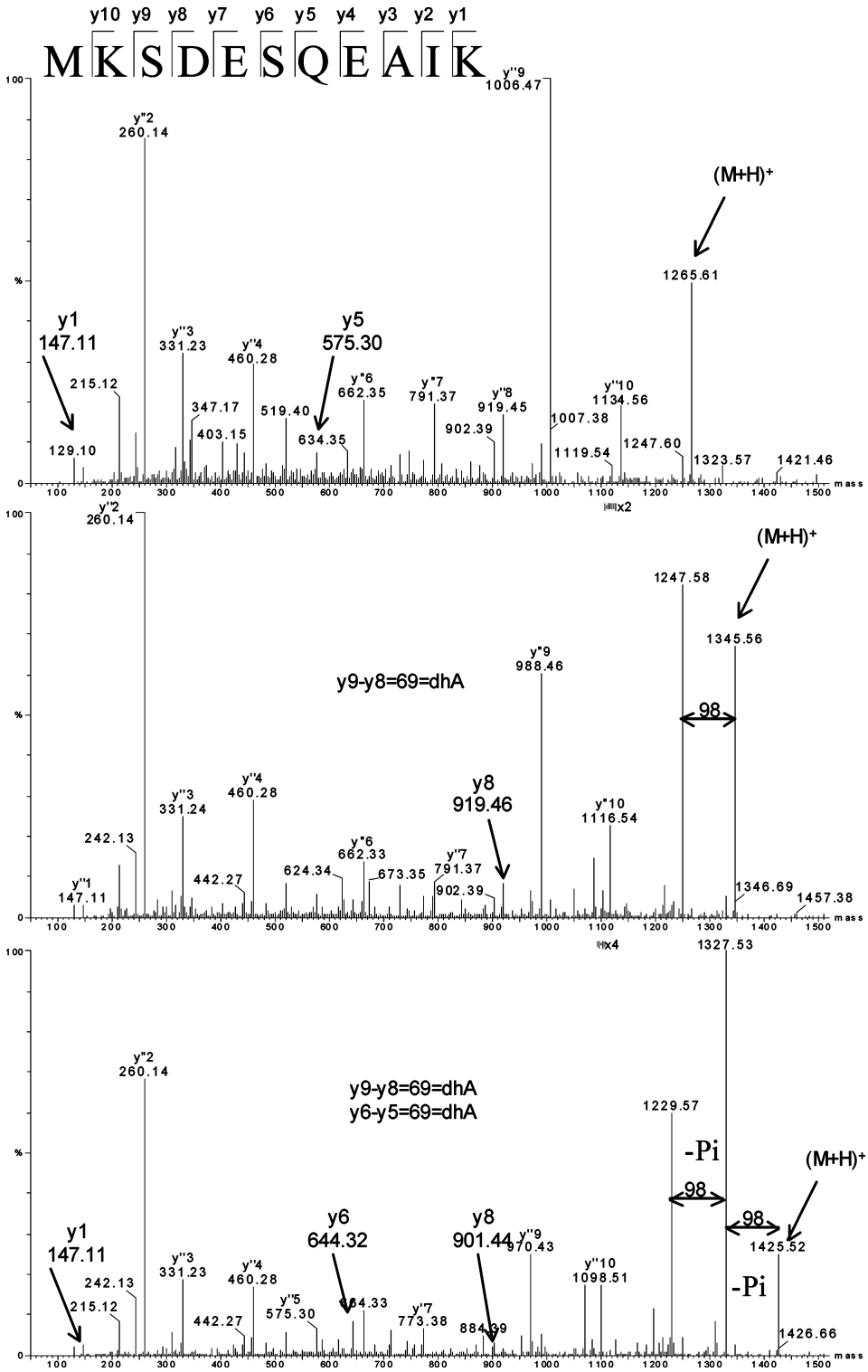

FIGURE 3: Tandem MS analysis of tryptic peptide MKSQESDEAIK. Processed CID MS/MS spectra from (top to bottom) unmodified OPN 162−172 (MKSQESDEAIK), monophosphorylated OPN 162−172 (MKpSQESDEAIK), and doubly phosphorylated OPN 162−172 (MKpSQEpSDEAIK). The loss of 98 from the precursor ion corresponds to the neutral loss of phosphate, while 69 between neighboring *y* ions indicates dehydroalanine, which arises from elimination of the phosphate from phosphoserine residues.

(1425.51) phosphates. From the sequence, it can be concluded that both serine residues are phosphorylated for the largest peptide. The MaxEnt3-processed CID spectra for the doubly charged parent ion for all observed forms of OPN 162−172 are shown in Figure 3. For clarity, only the *y* ions are labeled. The modified peptides show intense ions with one or two losses of 98 from the respective parent ions, which is characteristic of phosphoserine or phosphothreonine residues. For the single-phosphorylated precursor, a dehydroalanine residue ($y^9-y^8 = 69$) is observed predominantly for S164, indicating that this serine is preferentially phosphorylated in this peptide.

Initial analysis of the data was performed with MASCOT. Even when the reported scores were high, all potential phosphopeptides were verified manually. All peptides assigned were obtained with high-quality MS/MS data multiple

Table 3: Tandem MS of Peptides from the Tryptic Digest of Rat OPN and the Corresponding Phosphorylation Sites as well as Other Modifications

number	peptide sequence in rat bone OPN	modifications (site)
T1−14	LPVKVAEFGSSEEK	carbamyl (N term), carbamyl (K4)
T5−14	VAEFGSSEEK	unmodified
T5−19	VAEFGSSEEKAHYSK	unmodified, phosphorylation (S10, S11), carbamyl (K14)
T20−35	HSDAVATWLKPDPSQK	unmodified, carbamyl (K29)
T36−54	QNLLAPQNSVSSEETDDFK	pGlu(T36), phosphorylation (S46, S47)
T129−137	GDSLAYGLR	unmodified
T142−161	SFPVSDEQYPDATDEDLTSR	unmodified, phosphorylation (S146, T154, S160), sulfation (Y150)
T162−172	MKSQESDEAIK	unmodified, phosphorylation (S164, S167), oxidation (M162)
T162−179	MKSQESDEAIKVIPVAQR	phosphorylation (S164, S167), carbamyl (K172)
T164−172	SQESDEAIK	phosphorylation (S167)
T180−191	LSVPSSDQDSNGK	deamidation (N189)
T219−244	ASHESTEQSDAIDSAEKPDAIDSAER	phosphorylation (S220, S223, S232)
T245−255	SDAISSQASSK	unmodified
T256−283	ASLEHQSHEFHSHEDKLVLDPKSKEDDR	phosphorylation (S257, S262, S267, S278)
T272−279	LVLDPKSK	phosphorylation (S278)
T272−283	LVLDPKSKEDDR	phosphorylation (S278)
T278−286	S KEDDRYLK	phosphorylation (S278)
T280−286	EDDRYLK	unmodified
T287−301	FRISHELESSSSEVN	phosphorylation (S290, S295, S296, S297)
T289−301	ISHELESSSSEVN	phosphorylation (S290, S295, S296, S297)

Table 4: Tandem MS Peptides from the Asp-N Digest of Rat OPN and the Corresponding Phosphorylation Sites as well as Other Modifications

number	peptide sequence in rat bone OPN	modifications (site)
D1−21	LPVKVAEFGSSEEKAHYSKHS	phosphorylation (S10, S11), carbamylation (N term, K4)
D22−50	DAVATWLKPDPSQKQNLLAPQNSVSSEET	phosphorylation (S46, S47, T50)
D22−51	DAVATWLKPDPSQKQNLLAPQNSVSSEET	phosphorylation (S46, S47, T50)
D51−66	DDFKQETLPSNSNESH	phosphorylation (S60, S62, S65)
D130−146	DSLAYGLRSKSRSFPVS	unmodified, carbamylation (K139)
D130−154	DSLAYGLRSKSRSFPVSDEQYPDAT	phosphorylation (S146), sulfation (Y150)
D155−167	DEDLTSRMKSQES	unmodified
D157−167	DLTSRMKSQES	unmodified, phosphorylation (S164)
D168−184	DEAIKVIPVAQRLSVPS	unmodified
D168−186	DEAIKVIPVAQRLSVPSDQ	unmodified, carbamylation (K172)
D187−199	DSNGKTSHESSQL	deamidation (N189), phosphorylation (S193, S196)
D200−209	DEPSVETHSL	phosphorylation (S203)
D228−239	DAIDSAEKPDAI	phosphorylation (S232)
D237−245	DAIDSAERS	unmodified, phosphorylation (S241, S245)
D246−269	DAIDSQASSKASLEHQSHEFHSHE	phosphorylation (S257, S262, S267)
D249−269	DSQASSKASLEHQSHEFHSHE	phosphorylation (S257, S262, S267)
D281−301	DDRYLKFRISHELESSSSEVN	phosphorylation (S290, S295, S296, S297)

times to be considered high confidence. In several cases, the same phosphorylation sites were observed for both trypsin and Asp-N digests. These results are summarized in Tables 3 and 4. In all, 29 distinct phosphorylation sites were identified. The majority of these sites were found to be heterogeneous, and multiple sites could be identified even in the singly phosphorylated peptides. In OPN 51−66 (DDFKQETLPSNSNESH), it was determined that phosphorylation of S60 is always associated with phosphorylation of S62 and S65.

Other modifications were identified by MS/MS, and in some cases this complicated the identification of phosphorylated residues. For example, the N-terminal peptide, OPN 1−14, LPVKVAEFGSSEEK, was found to be carbamylated (+43) at the N terminus and K4, as well as phosphorylated. Carbamylation was also found on other residues. This is likely due to the urea used during the purification of OPN, despite deionization of urea solutions with mixed-bed resins prior to use. Other modifications that were observed include methionine oxidation (e.g., OPN 162−172), deamidation, and sulfation. The expected residue at position 189 is asparagine. However, in all instances of the corresponding peptides that were sequenced by MS/MS analysis in both enzymatic digests, an aspartic acid residue was determined for this position. This presumably arises from deamidation of asparagine. A total of 18 phosphorylation sites were identified in the trypsin digest and 25 in the Asp-N digest. Unique sites were found in each digest, giving a total of 29 identified phosphorylation sites in rat bone OPN.

Identification of Sulfation Site. The MS/MS spectrum of OPN 142−161 (SFPVSDEQYPDATDEDLTSR, *m*/*z* 1176.42 [1^+]) shows both a loss of 80 and a loss of 98 from the precursor ion. These could correspond to a loss of SO_3, indicating sulfation (*48*), or a loss of H_2PO_4, characteristic of phosphorylation (Figure 4). The *m*/*z* 1176.42 is also observed in the digest of dephosphorylated OPN. Tandem MS of the doubly charged peptide at *m*/*z* 1176.42 after phosphatase treatment shows that the parent peptide exhibits a loss of 80 Da (loss of *m*/*z* 40 for the 2^+ state) even with the low CE of 10 V. The modification is almost completely lost at a collision offset of 20 V, while the parent peptide is still present at 34 V prior to dephosphorylation (Figure 4). When these results are taken together, they strongly suggest that Y150 is sulfated. Examination using the Sulfinator tool (http://ca.expasy.org/tools/sulfinator/) (*49*) indicates that this is the only sulfation consensus sequence present in OPN.

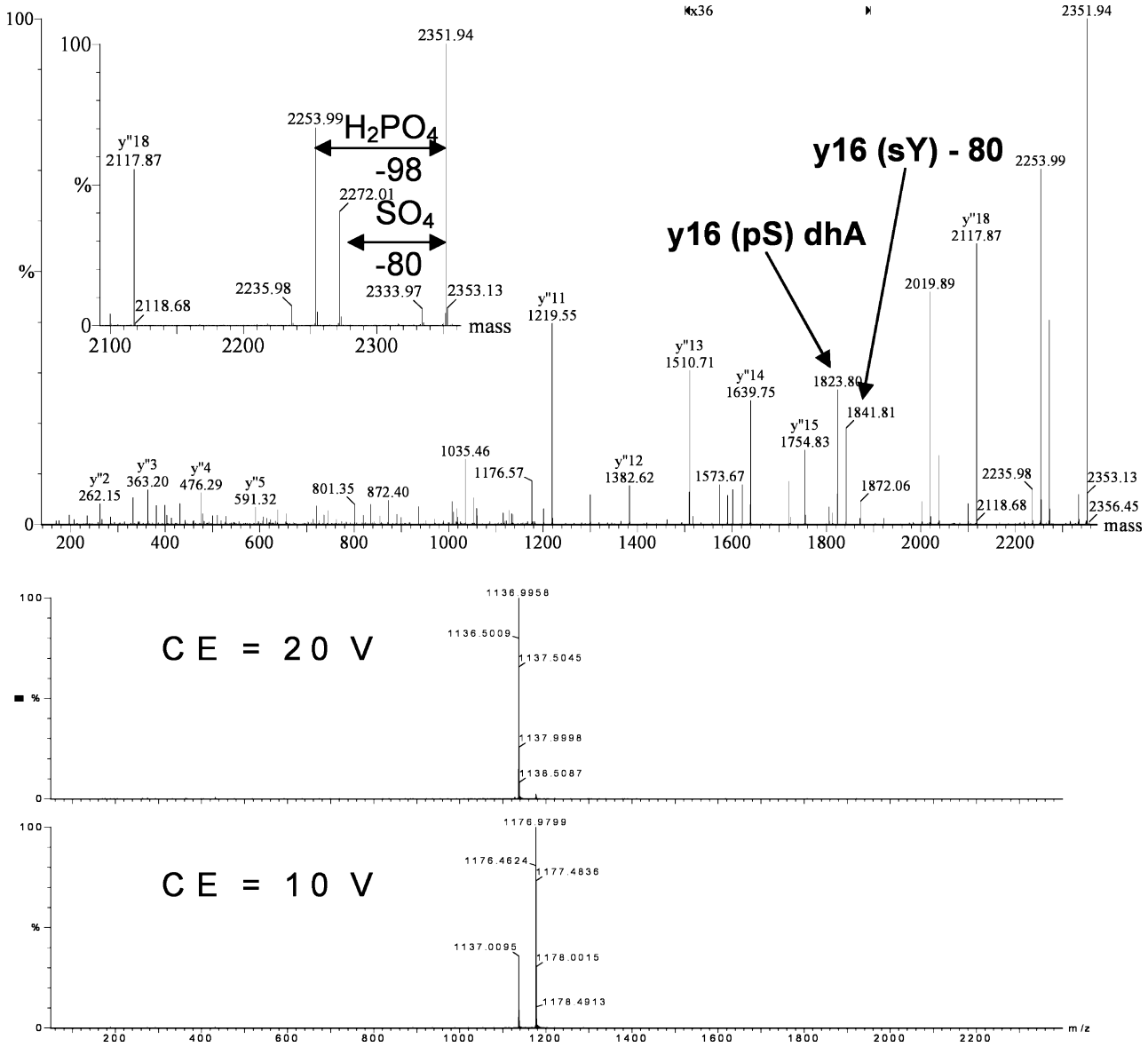

FIGURE 4: Tandem MS spectrum of a sulfated peptide. (A) MaxEnt3 processed MS/MS spectrum for 1176.42 (2^+) prior to enzymatic dephosphorylation. Data analysis shows that this corresponds to a mixture of SFPV**pS**DEQYPDATDEDLTSR and SFPVSDEQ**sY**PDATDEDLTSR. The loss of 80 and 98 are characteristic for sulfate and phosphate post-translation modification, respectively. (B) Raw data showing MS/MS of 1176.42 (2^+) after treatment with calf alkaline phosphatase. Loss of sulfate is exhibited even with the low collision offset of 10 V and almost completely lost at 20 V. For comparison, the MS/MS data in A was obtained using a CE of 34 V.

Glycan Analysis. No peptide species supporting N-linked glycosylation in OPN 51−66 (DDFKQETLPSNSNESH) were observed. As mentioned above, the region from D67−R128 was uncharacterized for phosphorylated OPN. This region is highly acidic, with 25 of the 62 residues being aspartic or glutamic acid. In the analogous region of bovine OPN, three of the four threonine residues are O-glycosylated, while the ESI−MS spectrum of dephosphorylated OPN suggests multiple sites of glycosylation. The region could be made more acidic by the presence of sialic acid located at the termini of *O*-glycans, a typical characteristic of this modification in mammals. The acidic nature of this region or the high *m*/*z* values expected for glycopeptides can explain the inability to detect this large peptide in the MS spectra obtained.

To simplify the glycan analysis, a tryptic digest of dephosphorylated rat bone OPN was treated with sialidase and used for LC−MS analysis. The raw and deconvoluted mass spectra of this digest show that the peptide corresponding to 55−128 (T6, theoretical *m*/*z* 8029.8) contains incremental additions of 365.3 Da ranging from four to eight disaccharide units of *N*-acetylhexosamine (*N*) and hexose (*H*) (HexNAc + Hex, *NH*). These results were further confirmed by observing the same addition of *NH* units on the larger peptide fragment corresponding to Q36−R128 (T5−T6, theoretical *m*/*z* 10 134.0). These results are summarized in Table 5.

To narrow down the location and structure of the glycans, these large tryptic peptides were further digested with Asp-N. Several glycopeptides from this digest were analyzed by MS/MS (Table 6). Glycosylation is indicated by the presence of diagnostic ions at *m*/*z* 204 and 366, corresponding to *H* and *NH* oxonium ions (*50*). Glycans were localized to individual threonine residues by manually analyzing the MS/MS data for glycopeptide-specific ions. An example of this is shown in Figure 5, which corresponds to the deconvoluted

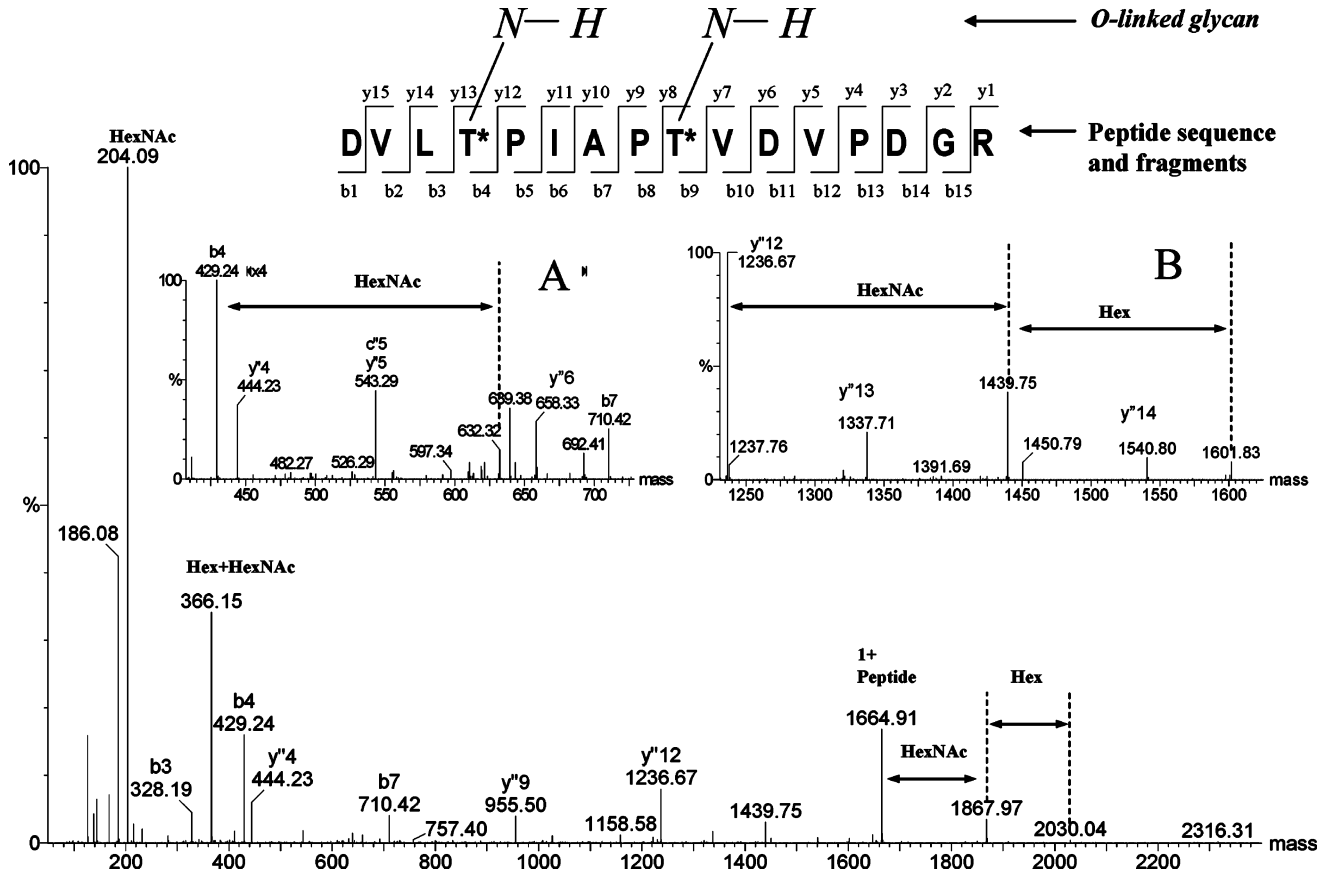

FIGURE 5: MS/MS analysis of glycopeptide related to DVLTPIAPTVDVPDGR. MaxEnt3 processed MS/MS spectrum for 799.08 (3^+) corresponding to the OPN 113−128 glycopeptide (DVLT*PIAPT*VDVPDGR) with two O-linked glycans (*NH*) at each threonine. Observed are singly charged peptide and glycopeptide fragments at *m*/*z* 429.24 (b4), 632.32 (b4 plus *N*), 794.3 (b4 plus *NH*), 1236.67 (y12), 1439.75 (y12 *N*), and 1601.83 (y12 plus *NH*) in embedded figures A and B that support O-linked glycosylation sites at T121 and T116. The deduced structure for each O-linked glycan is shown.

Table 5: Observed Masses for the Tryptic Glycopeptides Corresponding to OPN 55−128 (T6) and 36−128 (T5−T6) after Dephosphorylation and Desialylation

attached glycans		tryptic peptide			
		T6 MW (average): 8029.8 Da		T5−T6 MW (average): 10 134.0 Da	
composition	MW (average)	observed glycopeptide average mass	calculated mass	observed glycopeptide average mass (RI)	calculated mass
$(HN)_4$	1461.36	9491.5	9491.2	11 595.3	11 595.4
$(HN)_5$	1826.69	9855.5	9856.5	11 959.5	11 960.7
$(HN)_6$	2192.03	10 220.6	10 221.8	12 324.6	12 326.1
$(HN)_7$	2557.37	10 586.6	10 587.2	12 691.0	12 691.4
$(HN)_8$	2922.71	10 951.9	10 952.5	13 057.0	13 056.7

spectrum for OPN 113−128 (DVLTPIAPTVDVPDGR) with the glycans $(NH)_2$ attached (observed *m*/*z* 799.4 [3^+]). These data show that both T116 and T121 are glycosylated. Similarly, it was determined that both T107 and T110 are modified by *O*-glycans. Overall, the glycans were found to be heterogeneous with each threonine residue, having at least an attached *NH* moiety and at most the glycan $(NH)_2$ at each site for the species that we observed by MS.

Once analysis of the desialylated glycopeptides was in progress, attempts were made to study the dephosphorylated glycopeptides with sialic acid (*S*) present (i.e., no sialidase treatment). Signals for species corresponding to OPN 103−112 (DESFTASTQA) were not observed. However, two glycopeptides were observed at *m*/*z* 1077.8 (3^+) and 1199.5 (3^+). These correspond to OPN 113−125 (DVLTPIAPTVD-VP) with the addition of $(NH)_2S_4$, and $(NH)_3S_4$, respectively. Tandem MS of 1077.8 (3^+) (Figure 6) shows sialic-acid-containing fragments allowing structures to be assigned. A summary of the glycopeptide data is given in Table 6. Using all of the available data, the major glycan structure is thought to be $(NH)S_2$.

On the basis of the results shown in Table 6, it can be concluded that no phosphorylation of rat bone OPN occurs in the region D103−R128, a sequence not analyzed by tandem MS of the glycosylated protein (see above).

DISCUSSION

Phosphorylation Analysis. To determine the average number of phosphate groups present in rat bone OPN, the protein was treated with alkaline phosphatase and analyzed, together with untreated and recombinant OPN, by linear MALDI−TOF. The spectrum of untreated OPN gave a broad

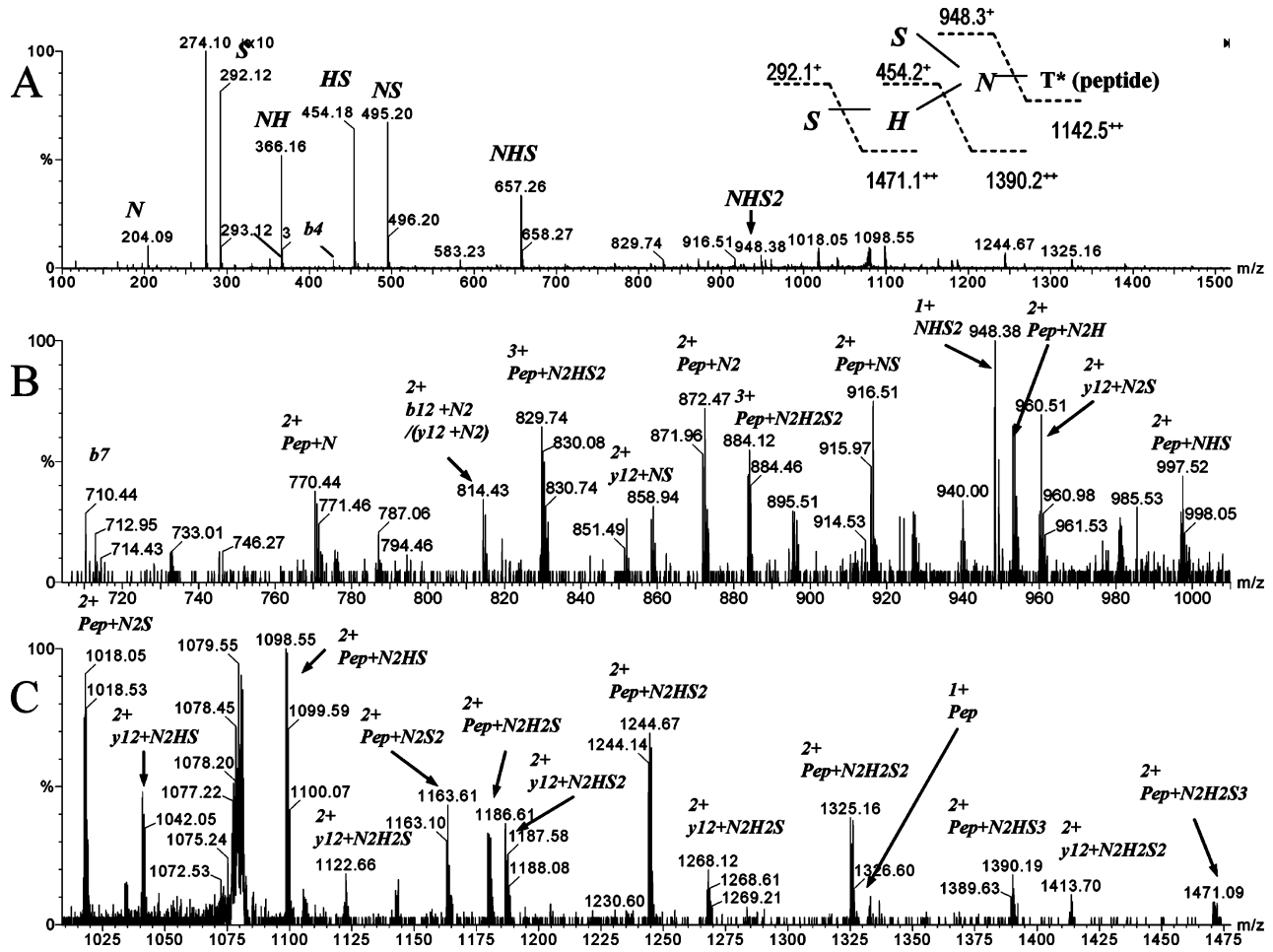

FIGURE 6: MS/MS analysis of glycopeptide related to DVLTPIAPTVDVP prior to sialidase treament. (A) Raw MS/MS spectrum of 1077.8 (3^+) corresponding to glycopeptide 113−125 (DVLT*PIAPT*VDVP) modified with $(NH)_2S_4$. (B and C) Expanded regions of A showing the glycan fragments in different mass ranges. Data support the structure given in Table 6 for which each threonine is modified with $(NH)S_2$.

peak centered at 37 621 Da, suggesting heterogeneity in phosphorylation and/or glycosylation. This mass is much lower than the value of 44 043 Da obtained by Prince and co-workers using sedimentation equilibrium ultracentrifugation (*41*). Because of its highly extended conformation (*51*), it is likely that OPN has a radius of gyration greater than that of a globular protein of equivalent molecular weight and therefore behaves anomalously in the ultracentrifuge. Therefore, the mass obtained by Prince and co-workers is probably an overestimate.

Phosphatase-treated OPN also gave a broad peak, centered at 36 790 Da, indicating that the heterogeneity is likely due to the presence of carbohydrate. The mass difference between phosphatase-treated and -untreated OPN species, 831 Da, corresponds to 10.4 phosphates. Prince and co-workers reported that rat bone OPN contains 13.25 mol of phosphate/mol of protein (*41*). However, this was based on a molecular mass of 44 kDa; using a mass of 37.6 kDa reduces the phosphate content to 11.3 mol/mol of protein.

The present analysis confirms 6 of the 7 phosphorylation sites positively identified in rat bone OPN by Neame and Butler (S10, S11, S46, S47, S295, and S297 but not S298) and 4 of the 5 sites "likely" phosphorylated (T154, S160, S257, and S262 but not S250) (*37*) (Figure 7). Three of our sites (S10, S11, and S60) correspond to residues phosphorylated in chicken bone OPN (S14, S15, and S59) (*52*). The other 5 phosphorylated residues found in chicken OPN (S12, S58, T155, S196, and S215) are not conserved in rat OPN (F8, P59, K163, D246, and F265).

Of the 29 phosphoserine and phosphothreonine residues that we identified, 17 are present at the corresponding positions in bovine milk OPN (see Figure 7). Residues phosphorylated in bovine milk OPN were generally phosphorylated or not conserved in the rat bone isoform. The exceptions (rat S44, S84, S93, S99, S102, S208, and S250) mostly occurred in the region for which we were unable to identify phosphorylation sites (67−102).

It is not known with certainty which enzyme(s) is responsible for the phosphorylation of OPN *in vivo*. Salih found that protein kinase CK2 adds more phosphate to OPN than either cGMP-dependent protein kinase or protein kinase C (*53*). However, others have reported that Golgi casein kinase is responsible for all or most of OPN phosphorylation (*36*, *54*). It has also been claimed that a substantial amount of phosphate is added to OPN extracellularly (*55*, *56*). Other enzymes associated with the phosphorylation of OPN include cAMP-dependent protein kinase (*57*) and protein kinase CK1 (*54*). Of the 29 sites of phosphorylation that we have identified in rat bone OPN, only 10 are located in the canonical consensus sequence (S/TxxD/E/pS/pT) for protein kinase CK2, whereas 25 are in the canonical consensus sequence for Golgi casein kinase (S/TxD/E/pS/pT). Of the

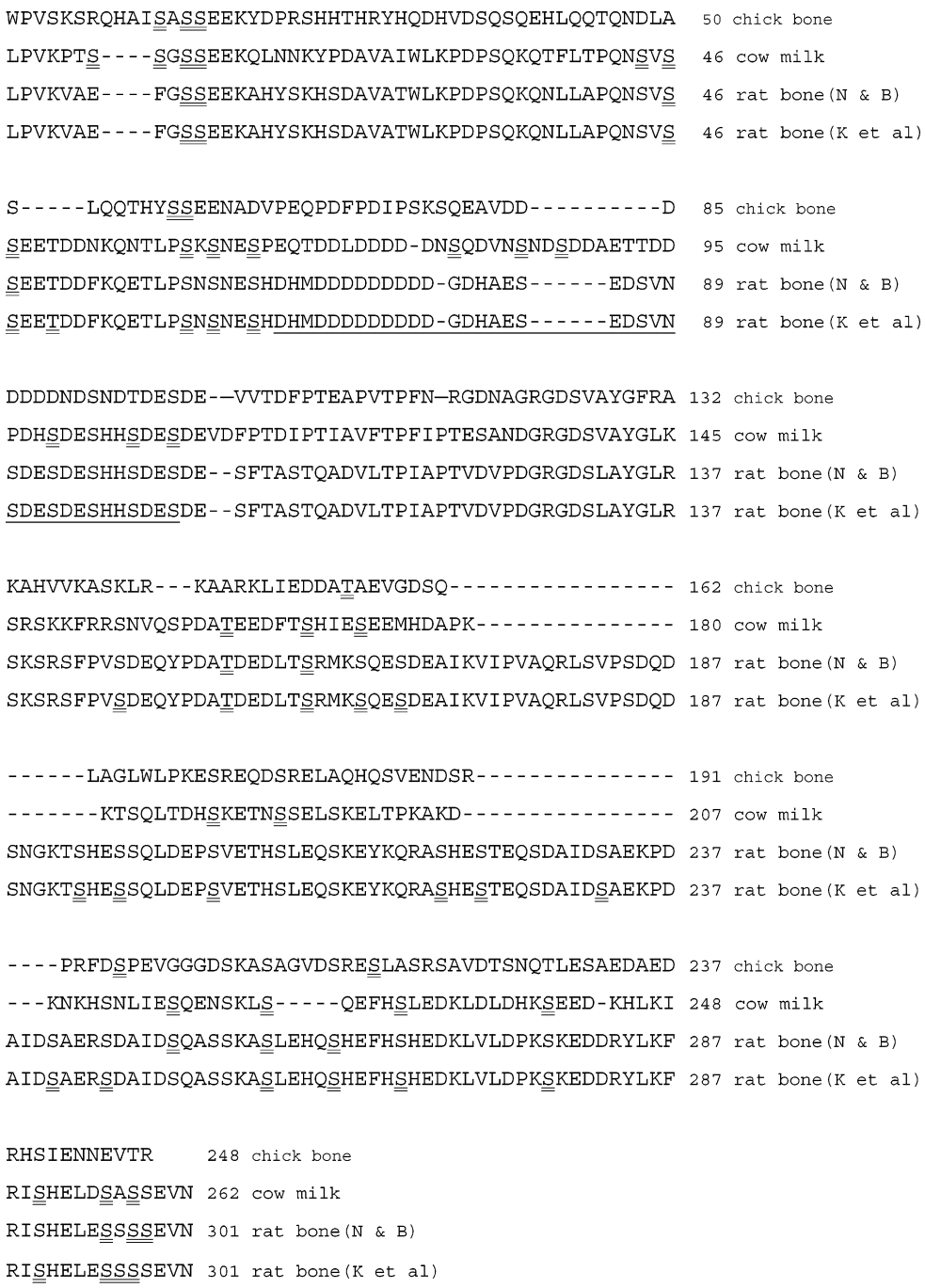

FIGURE 7: Comparison of phosphorylation sites in rat bone, chick bone, and cow milk isoforms of OPN. Sequences were obtained from SwissProt and aligned using Clustal W. Phosphorylated residues are double-underlined. Chick bone data are from Salih et al. (*52*); cow milk data are from Sørensen et al. (*36*); and rat bone data are from Neame and Butler (*37*) and from the present study. The sequence not analyzed for phosphorylation in the present study is single-underlined.

latter group, the great majority (*21*) are in the sequence S/TxE. Three phosphorylated serines, S160, S196, and S245, occur in neither canonical sequence, although S196 is in an alternative recognition sequence for Golgi casein kinase (*58*). CK2 is known to act on many sequences other than the canonical one, including sites corresponding to the Golgi casein kinase consensus sequence (*59*). However, we have found only 8 phosphorylated residues in recombinant rat OPN treated with CK2 (M. Keykhosravani, unpublished results). Our findings are therefore consistent with the view that Golgi casein kinase is primarily responsible for OPN phosphorylation *in vivo*, but in view of the promiscuous nature of these enzymes it is difficult to draw a definitive conclusion on this point.

Rat OPN contains 39 more amino acids than cow OPN. The 36-residue sequence (67−102) that we were unable to characterize for phosphorylated OPN contains 7 serines and no threonines. It is highly likely that some of these serines are phosphorylated: four occur in SxE sequences, the most common phosphorylated motif in OPN. Also, the sequence in cow milk OPN corresponding to rat OPN 67−102 contains 6 sites of phosphorylation (*36*). Therefore, the number of sites of phosphorylation in rat bone OPN is probably significantly higher than that in the bovine milk isoform.

Table 6: Observed *m/z* for Glycopeptides Observed after and prior to Sialidase Treatment[a]

Peptide (monoisotopic mass)	Observed m/z (charge state)	Glycan Composition	Structures Observed
DESFT*AST*QA (MW=1055.44)	893.8 (2+)	$(NH)_2$	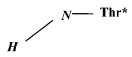
	1076.9 (2+)	$(NH)_3$	
	1259.5 (2+)	$(NH)_4$	
FT*AST*QA (MW=724.34)	728.3 (2+)	$(NH)_2$	
	910.9 (2+)	$(NH)_3$	
	1094.5 (2+)	$(NH)_4$	
DVLT*PIAPT*VDVP (MW=1335.73)	1034.0 (2+)	$(NH)_2$	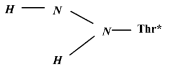
	1217.1 (2+)	$(NH)_3$	
DVLT*PIAPT*VDVPDGR (MW=1663.88)	799.4 (3+)	$(NH)_2$	
	1198.6 (2+)		
	921.1 (3+)	$(NH)_3$	
	1042.9 (3+)	$(NH)_4$	
DV LT*PIAPT*VDV P (before sialidase) (MW=1335.73)	1077.8 (3+)	$(NH)_2S_4$	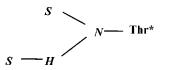
	1199.5 (3+)	$(NH)_3S_4$	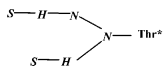

[a] Analysis of the corresponding MS/MS data supports the major structures given.

However, it is clear that the average level of phosphorylation of bone OPN is much lower than that of the milk isoform. On the basis of the 29 phosphorylation sites identified in the present study, the average efficiency of phosphorylation is approximately 36%. Adding (conservatively) 4 sites for the 36-residue sequence not analyzed, the average efficiency is probably no higher than 32%. In chicken bone OPN, the average phosphate content per phosphorylated site has been measured as 53% (*52*). It is not clear whether some serines and threonines are phosphorylated to a higher degree than others.

Sulfation. Sulfation of OPN has previously been detected by metabolic labeling with $^{35}SO_4$ (*43*, *60*) but was not localized. All of the current MS evidence supports sulfation of rat bone OPN at Y150 (see Figure 4), which is in the vicinity of the RGD motif (residues 128−130). The degree of sulfation cannot be determined in positive-ion-mode ESI−MS. Y150 of rat OPN is conserved in mouse, human, and rabbit but not in pig, cow, sheep, or chicken. Therefore, sulfation of OPN may be species-dependent.

For most sulfated proteins, no functional role has been attributed to this post-translational modification. In human bone sialoprotein, the presence of two sulfotyrosine residues close to the RGD motif led to the speculation that sulfation may be involved in integrin binding (*61*). In this case, however, the sulfation and cell-binding sites are in closer proximity than in rat bone OPN.

N-Linked Glycans. The difference in mass between the OPN polypeptide and alkaline phosphatase-treated bone OPN, 3543 Da, can presumably all be accounted for by carbohydrate, the sulfate group, and phosphate groups not susceptible to alkaline phosphatase. Between the tryptic and Asp-N peptides of phosphorylated rat bone OPN, we achieved coverage of the entire molecule except the 62-residue sequence 67−128. The failure to detect this peptide appears to be due to the presence of several glycan chains.

There is only one consensus sequence for N-glycosylation (NxS) in rat OPN. The corresponding peptide from AspN digestion (51−66, DDFKQETLPSNSNESH, Table 4) is phosphorylated with no evidence for N-glycosylation. This is consistent with earlier work showing that OPN secreted by rat kidney cells (*62*) and rat fibroblasts (*42*) is not N-glycosylated. Prince and co-workers' suggestion that rat bone OPN contains one N-linked glycan was based only on the presence of mannose in hydrolyzates of the protein (*41*). Human bone OPN contains a single N-linked oligosaccharide of 2302 Da (*63*), but because the site of glycosylation was not identified, it is not known whether the asparagine residue involved is conserved in rat.

O-Linked Glycans. In this study, rat OPN has been shown to contain 4 O-linked glycans. All of the residues that are glycosylated are threonine (T107, T110, T116, and T121). Of these, all but T110 are conserved in other OPNs. The threonines corresponding to T107, T116, and T121 of rat OPN carry the three *O*-glycans of the bovine milk isoform (*36*). In work performed on the tsB77 cell line, evidence supports the presence of sialic acid on all of the O-linked glycans, with these being required for cell-surface binding (*42*). It appears that sialic acid is present for all of the O-linked glycans that we found.

In conclusion, a comprehensive analysis of rat bone OPN has identified 29 phosphorylation sites, 19 of which have not been described previously, 1 sulfation site, and 4 O-linked glycans. A total of 25 of the phosphorylated residues are in consensus sequences for Golgi casein kinase. It is likely that some of these novel phosphorylation sites contribute to the crystal-inhibiting and osteoclast-activating properties of the protein. Further studies are necessary to identify the functional significance of individual phosphate groups as well as the sulfate group and O-linked glycans of rat bone OPN.

REFERENCES

1. Senger, D. R., Wirth, D. F., and Hynes, R. O. (1979) Transformed mammalian cells secrete specific proteins and phosphoproteins, *Cell 16*, 885−893.
2. Franzén, A., and Heinegård, D. (1985) Isolation and characterization of two sialoproteins present only in bone calcified matrix, *Biochemistry 232*, 715−724.
3. Oldberg, A., Franzén, A., and Heinegård, D. (1986) Cloning and sequence analysis of rat bone sialoprotein (osteopontin) cDNA reveals an Arg-Gly-Asp cell-binding sequence, *Proc. Natl. Acad. Sci. U.S.A. 83*, 8819−8823.
4. Craig, A. M., Smith, J. H., and Denhardt, D. T. (1989) Osteopontin, a transformation-associated cell adhesion phosphoprotein, is induced by 12-*O*-tetradecanoylphorbol 13-acetate in mouse epidermis, *J. Biol. Chem. 264*, 9682−9689.
5. Giachelli, C. M., and Steitz, S. (2000) Osteopontin: A vesatile regulator of inflammation and biomineralization, *Matrix Biol. 19*, 615−622.
6. Denhardt, D. T., Giachelli, C. M., and Rittling, S. R. (2001) Role of osteopontin in cellular signalling and toxicant injury, *Annu. Rev. Pharmacol. Toxicol. 41*, 723−749.
7. Senger, D. R., Perruzzi, C. A., Papadopoulos, A., and Tenen, D. G. (1989) Purification of human milk protein closely similar to

tumor-secreted phosphoproteins and osteopontin, *Biochim. Biophy. Acta 996*, 43−48.
8. O'Regan, A., and Berman, J. S. (2000) Osteopontin: A key cytokine in cell-mediated and granulomatous inflammation, *Int. J. Exp. Pathol. 81*, 373−390.
9. Weber, G. F., Ashkar, S., Glimcher, M. J., and Cantor, H. (1996) Receptor−ligand interaction between CD44 and osteopontin (Eta-1), *Science 271*, 509−512.
10. Takahashi, F., Takahashi, K., Maeda, K., Tominaga, S., and Fukuchi, Y. (2000) Osteopontin is induced by nitric oxide in RAW 264.7 cells, *IUBMB Life 49*, 217−221.
11. Denhardt, D. T., Noda, M., O'Regan, A. W., Pavlin, D., and Berman, J. S. (2001) Osteopontin as a means to cope with environmental insults: Regulation of inflammation, tissue remodelling, and cell survival, *J. Clin. Invest. 107*, 1055−1061.
12. Gardner, H. A., Berse, B., and Senger, D. R. (1994) Specific reduction in osteopontin synthesis by antisense RNA inhibits the tumorigenicity of transformed Rat1 fibroblasts, *Oncogene 9*, 2321−2326.
13. Sung, V., Gilles, C., Murray, A., Clarke, R., Aaron, A. D., Azumi, N., and Thompson, E. W. (1998) The LCC15-MB human breast cancer cell line expresses osteopontin and exhibits an invasive and metastatic phenotype, *Exp. Cell Res. 241*, 273−284.
14. Chambers, A. F., Hota, C., and Prince, C. W. (1993) Adhesion of metastatic, ras-transformed NIH 3T3 cells to osteopontin, fibronectin, and laminin, *Cancer Res. 53*, 701−706.
15. Oates, A. J., Barraclough, R., and Rudland, P. S. (1996) The identification of osteopontin as a metastasis-related gene product in a rodent mammary tumour model, *Oncogene 13*, 97−104.
16. Ross, F. P., Chappel, J., Alvarez, J. I., Sander, D., Butler, W. T., Farach-Carson, M. C., Mintz, K. A., Robey, P. G., Teitelbaum, S. L., and Cheresh, D. A. (1993) Interactions between the bone matrix proteins osteopontin and bone sialoprotein and the osteoclast integrin $\alpha_v\beta_3$ potentiate bone resorption, *J. Biol. Chem. 268*, 9901−9907.
17. Yamate, T., Mocharla, H., Taguchi, Y., Igietseme, J. U., Manolagas, S. C., anad Abe, E. (1997) Osteopontin expression by osteoclast and osteoblast progenitors in the murine bone marrow: Demonstration of its requirements for osteoclastogenesis and its increase after ovariectomy, *Endocrinology 138*, 3047−3055.
18. Giachelli, C. M., Bae, N., Almeida, M., Denhardt, D. T., Alpers, C. E., and Schwartz, S. M. (1993) Osteopontin is elevated during neointima formation in rat arteries and is a novel component of human atherosclerotic plaques, *J. Clin. Invest. 92*, 1686−1696.
19. Kohri, K., Nomura, S., Kitamura, Y., Nagata, T., Yoshioka, K., Iguchi, M., Yamate, T., Umekawa, T., Suzuki, Y., Sinohara, H., and Kurita, T. (1993) Structure and expression of the mRNA encoding urinary stone protein (osteopontin), *J. Biol. Chem. 268*, 15180−15184.
20. Kido, J., Kasahara, C., Ohishi, K., Nishikawa, S., Ishida, H., Yamashita, K., Kitamura, S., Kohri, K., and Nagata, T. (1995) Identification of osteopontin in human dental calculus matrix, *Arch. Oral Biol. 40*, 967−972.
21. Bellahcene, A., and Castronovo, V. (1997) Expression of bone matrix proteins in human breast cancer: Potential roles in microcalcification formation and in the genesis of bone metastases, *Bull. Cancer 84*, 17−24.
22. Boskey, A. L., Maresca, M., Ullrich, W., Doty, S. B., Butler, W. T., and Prince, C. W. (1993) Osteopontin−hydroxyapatite interactions *in vitro*. Inhibition of hydroxyapatite formation and growth in a gelatin-gel, *Bone Miner. 22*, 147−159.
23. Hunter, G. K., Kyle, C. L., and Goldberg, H. A. (1994) Modulation of crystal formation by bone phosphoproteins: Structural specificity of the osteopontin-mediated inhibition of hydroxyapatite formation, *Biochem. J. 300*, 723−728.
24. Hunter, G. K., Hauschka, P. V., Poole, A. R., Rosenberg, L. C., and Goldberg, H. A. (1996) Nucleation and inhibition of hydroxyapatite formation by mineralized tissue proteins, *Biochem. J. 317*, 59−64.
25. Shiraga, H., Min, W., van Dusen, W. J., Clayman, M. D., Miner, D., Terrell, C. H., Sherbotie, J. R., Foreman, J. W., Przysiecki, C., Nielson, E. G., and Hoyer, J. R. (1992) Inhibition of calcium oxalate crystal growth *in vitro* by uropontin: Another member of the aspartic acid-rich protein superfamily, *Proc. Natl. Acad. Sci. U.S.A. 89*, 426−430.
26. Worcester, E. M., Blumenthal, S. S., Beshensky, A. M., and Lewand, D. L. (1992) The calcium oxalate crystal growth inhibitor protein produced by mouse kidney cortical cells in culture is osteopontin, *J. Bone Miner. Res. 7*, 1029−1036.
27. Hincke, M. T., and St. Maurice, M. (2000) in *The Chemistry and Biology of Mineralized Tissues* (Goldberg, M., Boskey, A., and Robinson, C., Eds.) pp 13−17, American Academy of Orthopaedic Surgeons, Rosemont, IL.
28. Jono, S., Peinado, C., and Giachelli, C. M. (2000) Phosphorylation of osteopontin is required for inhibition of vascular smooth muscle cell calcification, *J. Biol. Chem. 275*, 20197−20203.
29. Hoyer, J. R., Asplin, J. R., and Otvos, L. (2001) Phosphorylated osteopontin peptides suppress crystallization by inhibiting the growth of calcium oxalate crystals, *Kidney Int. 60*, 77−82.
30. Pampena, D. A., Robertson, K. A., Litvinova, O., Lajoie, G., Goldberg, H. A., and Hunter, G. K. (2004) Inhibition of hydroxyapatite formation by osteopontin phosphopeptides, *Biochem. J. 378*, 1083−1087.
31. Katayama, Y., House, C. M., Udagawa, N., Kazama, J. J., McFarland, R. J., Martin, T. J., and Findlay, D. M. (1998) Casein kinase 2 phosphorylation of recombinant rat osteopontin enhances adhesion of osteoclasts but not osteoblasts, *J. Cell. Phys. 176*, 179−187.
32. Ek-Rylander, B., Florest, M., Wendel, M., Heinegård, D., and Andersson, G. (1994) Dephosphorylation of osteopontin and bone sialoprotein by osteoclastic tartrate-resistant acid phosphatase, *J. Biol. Chem. 269*, 14853−14856.
33. Razzouk, S., Brunn, J. C., Qin, C., Tye, C. E., Goldberg, H. A., and Butler, W. T. (2002) Osteopontin posttranslational modifications, possibly phosphorylation, are required for *in vitro* bone resorption but not osteoclast adhesion, *Bone 30*, 40−47.
34. Weber, G. F., Zawaideh, S., Hikita, S., Kumar, V. A., Cantor, H., and Ashkar, S. (2002) Phosphorylation-dependent interaction of osteopontin with its receptors regulates macrophage migration and activation, *J. Leukocyte Biol. 72*, 752−761.
35. Ashkar, S., Weber, G. F., Panoutsakopoulou, V., Sanchirico, M. E., Jansson, M., Zawaideh, S., Rittling, S. R., Denhardt, D. T., Glimcher, M. J., and Cantor, H. (2000) Eta-1 (osteopontin): An early component of type-1 (cell-mediated) immunity, *Science 287*, 860−864.
36. Sørensen, E. S., Højrup, P., and Petersen, T. E. (1995) Posttranslational modifications of bovine osteopontin: Identification of twenty-eight phosphorylation and three O-glycosylation sites, *Protein Sci. 4*, 2040−2049.
37. Neame, P. J., and Butler, W. T. (1996) Posttranslational modification in rat bone osteopontin, *Connect. Tissue Res. 35*, 145−150.
38. Nemir, M., DeVouge, M. W., and Mukherjee, B. B. (1989) Normal rat kidney cells secrete both phosphorylated and nonphosphorylated forms of osteopontin showing different physiological properties, *J. Biol. Chem. 264*, 18202−18208.
39. Sodek, J., Chen, J., Nagata, T., Kasugai, S., Todescan, R., Li, I. W. S., and Kim, R. H. (1995) Regulation of osteopontin expression in osteoblasts, *Ann. N. Y. Acad. Sci. 760*, 223−241.
40. Safran, J. B., Butler, W. T., and Farach-Carson, M. C. (1998) Modulation of osteopontin post-translational state by 1,25-$(OH)_2$-vitamin D_3. Dependence on Ca^{2+} influx, *J. Biol. Chem. 273*, 29935−29941.
41. Prince, C. W., Oosawa, T., Butler, W. T., Tomana, M., Bhown, A. S., Bhown, M., and Schrohenloher, R. E. (1987) Isolation, characterization, and biosynthesis of phosphorylated glycoprotein from rat bone, *J. Biol. Chem. 262*, 2900−2907.
42. Shanmugam, V., Chackalaparampil, I., Kundu, G. C., Mukherjee, A. B., and Mukherjee, B. B. (1997) Altered sialylation of osteopontin prevents its receptor-mediated binding on the surface of oncogenically transformed tsB77 cells, *Biochemistry 36*, 5729−5738.
43. Nagata, T., Todescan, R., Goldberg, H. A., Zhang, Q., and Sodek, J. (1989) Sulphation of secreted phosphoprotein I (SPPI, osteopontin) is associated with mineralized tissue formation, *Biochem. Biophys. Res. Commun. 165*, 234−240.
44. Goldberg, H. A., and Sodek, J. (1994) Purification of mineralized tissue-associated osteopontin, *J. Tissue Cult. Methods 16*, 211−215.
45. Goldberg, H. A., and Warner, K. J. (1997) The staining of acidic proteins on polyacrylamide gels: Enhanced sensitivity and stability of "Stains-All" staining in combination with silver nitrate, *Anal. Biochem. 251*, 227−233.
46. Ferrige, A. G., Seddon, M. J., Green, B. N., Jarvis, S. A., and Skilling, J. (1992) Disentangling electrospray spectra with maximum entropy, *Rapid Comm. Mass Spectrom. 6*, 707−711.
47. Ma, B., Zhang, K., Hendrie, C., Liang, C., Li, M., Doherty-Kirby, A., and Lajoie, G. (2003) PEAKS: Powerful software for peptide

de novo sequencing by tandem mass spectrometry, *Rapid Commun. Mass Spectrom. 17*, 2337−2342.
48. Onnerfjord, P., Heathfield, T. F., and Heinegard, D. (2004) Identification of tyrosine sulfation in extracellular leucine-rich repeat proteins using mass spectrometry, *J. Biol. Chem. 279*, 26−33.
49. Monigatti, F., Gasteiger, E., Bairoch, A., and Jung, E. (2002) The Sulfinator: Predicting tyrosine sulfation sites in protein sequences, *Bioinformatics 18*, 769−770.
50. Zhang, C. J., Doherty-Kirby, A., van Huystee, R., and Lajoie, G. (2004) Investigation of cationic peanut peroxidase glycans by electrospray ionization mass spectrometry, *Phytochemistry 65*, 1575−1588.
51. Fisher, L. W., Torchia, D. A., Fohr, B., Young, M. F., and Fedarko, N. S. (2001) Flexible structures of SIBLING proteins, bone sialoprotein, and osteopontin, *Biochem. Biophys. Res. Comm. 280*, 460−465.
52. Salih, E., Ashkar, S., Gerstenfeld, L. C., and Glimcher, M. J. (1997) Identification of the phosphorylated sites of metabolically ^{32}P-labeled osteopontin from cultured chicken osteoblasts, *J. Biol. Chem. 272*, 13966−13973.
53. Salih, E., Ashkar, S., Zhou, H. Y., Gerstenfeld, L., and Glimcher, M. J. (1996) Protein kinases of cultured chicken osteoblasts that phosphorylate extracellular bone proteins, *Connect. Tissue Res. 35*, 207−213.
54. Lasa, M., Chang, P. L., Prince, C. W., and Pinna, L. A. (1997) Phosphorylation of osteopontin by Golgi apparatus casein kinase, *Biochem. Biophys. Res. Comm. 240*, 602−605.
55. Suzuki, Y., Kubota, T., Koizumi, T., Satoyoshi, M., Teranaka, T., Kawase, T., Ikeda, T., Yamaguchi, A., Saito, S., and Mikuni-Takagaki, Y. (1996) Extracellular processing of bone and dentin proteins in matrix mineralization, *Connect. Tissue Res. 35*, 223−229.
56. Zhu, X., Luo, C., Ferrier, J. M., and Sodek, J. (1997) Evidence of ectokinase-mediated phosphorylation of osteopontin and bone sialoprotein by osteoblasts during bone formation *in vitro*, *Biochem. J. 323* (part 3), 637−643.
57. Ashkar, S., Teplow, D. B., Glimeher, M. J., and Saavedra, R. A. (1993) *In vitro* phosphorylation of mouse osteopontin expressed in *E. coli*, *Biochem. Biophys. Res. Comm. 191*, 126−133.
58. Brunati, A. M., Marin, O., Bisinella, A., Salviati, A., and Pinna, L. A. (2000) Novel consensus sequence for the Golgi apparatus casein kinase, revealed using proline-rich protein-1 (PRP1)-derived peptide substrates, *Biochem. J. 351*, 765−768.
59. Meggio, F., and Pinna, L. A. (2003) One-thousand-and-one substrates of protein kinase CK2? *FASEB J. 17*, 349−368.
60. Ecarot-Charrier, B., Bouchard, F., and Delloye, C. (1989) Bone sialoprotein II synthesized by cultured osteoblasts contains tyrosine sulfate, *J. Biol. Chem. 264*, 20049−20053.
61. Zaia, J., Boynton, R., Heinegard, D., and Barry, F. (2001) Posttranslational modifications to human bone sialoprotein determined by mass spectrometry, *Biochemistry 40*, 12983−12991.
62. Singh, K., DeVouge, M. W., and Mukherjee, B. B. (1990) Physiological properties and differential glycosylation of phosphorylated and nonphosphorylated forms of osteopontin secreted by normal rat kidney cells, *J. Biol. Chem. 265*, 18696−18701.
63. Masuda, K., Takahashi, N., Tsukamoto, Y., Honma, H., and Kohri, K. (2000) *N*-Glycan structure of an osteopontin from human bone, *Biochem. Biophys. Res. Comm. 268*, 814−817.

BI050109P